

Journal of Materials Chemistry A

Accepted Manuscript



This is an *Accepted Manuscript*, which has been through the Royal Society of Chemistry peer review process and has been accepted for publication.

Accepted Manuscripts are published online shortly after acceptance, before technical editing, formatting and proof reading. Using this free service, authors can make their results available to the community, in citable form, before we publish the edited article. We will replace this *Accepted Manuscript* with the edited and formatted *Advance Article* as soon as it is available.

You can find more information about *Accepted Manuscripts* in the [Information for Authors](#).

Please note that technical editing may introduce minor changes to the text and/or graphics, which may alter content. The journal's standard [Terms & Conditions](#) and the [Ethical guidelines](#) still apply. In no event shall the Royal Society of Chemistry be held responsible for any errors or omissions in this *Accepted Manuscript* or any consequences arising from the use of any information it contains.

Sandwich structured PVdF/PMIA/PVdF nanofibrous separators with robust mechanical strength and thermal stability for lithium ion battery

Cite this: DOI: 10.1039/x0xx00000x

Received 00th January 2012,
Accepted 00th January 2012

DOI: 10.1039/x0xx00000x

www.rsc.org/

Yunyun Zhai,^{ab} Na Wang,^a Xue Mao,^a Yang Si,^a Jianyong Yu,^c Salem S. Al-Deyab,^d Mohamed El-Newehy,^{de} and Bin Ding^{*ac}

Novel, sandwich structured PVdF/PMIA/PVdF nanofibrous battery separators with robust mechanical strength and thermal stability are fabricated via a sequential electrospinning technique. The nanofibers of the PVdF and the PMIA layers are bonded and interconnected on the interface boundary without any polymer binder and post-treatment. Benefiting from the high porosity of the as-prepared membranes and the introduction of PMIA, the PVdF/PMIA/PVdF composite membranes exhibit high ionic conductivity (2.3 times higher than that of the Celgard membrane), robust tensile strength (13.96 MPa), and excellent thermal stability to sustain the insulation after closing the pores in the PVdF layer. Hot oven test reveals that the composite membranes exhibit no dimension shrinkage after being exposed to 180 °C for 1 h. Furthermore, the as-prepared membranes based Li/LiCoO₂ cell shows higher capacity retention of 93.10% after 100 cycles and better rate property compared with the cell using Celgard membrane, providing a new insight into the design and development of high performance rechargeable lithium ion batteries.

Introduction

Lithium secondary batteries have stimulated extensive interest due to their wide applications in smart electronic devices, plug-in hybrid electric vehicles and grid energy storage system.^{1,2} Nowadays, the safety of lithium ion battery has become a persisting problem and caused a serious danger to human body, such as the Boeing B747-400F cargo plane catch fire.³ Cell separator, a thin membrane that keeps the positive and negative electrodes apart and allows rapid transport of ionic charge carrier, is considered to be one of the most important part that concerns the safety of lithium ion battery.^{4,5} Currently, the most widely used separators of lithium ion secondary batteries are mainly composed of polythene (PE), polypropylene (PP), and PE/PP composites.^{6,7} Although these separators provide relatively high mechanical strength and thermal shutdown property, most of them suffer from low porosity of less than 50%, poor wettability in liquid electrolytes, and unsatisfactory thermal stability.^{8,9} Until now, tremendous efforts have been devoted to overcome these limitations, such as modification of polyolefin with ceramic powders and/or other polymers,^{10,11} the introduction of nonwoven-based composite separators,¹² and

other fabrication techniques.^{13,14} However, there still remain a lot of limitations for practical applications because of costly and complicated fabrication procedures and weak bonding force between the matrix and the modifier. Without doubt, there is a great need for further development of new separators with high performance.

Electrospinning has been widely used as an attractive method to prepare a wide variety of functional fibrous membranes with controllable compositions and structures.¹⁵⁻¹⁸ Electrospun nanofibrous membranes possess interconnected porous structure, high porosities and air permeability, thus they are able to uptake large amounts of liquid electrolytes and offer effective conduction channels, which in turn brings high ionic conductivity and good electrochemical property.¹⁹ Based on these characteristics, nanofiber-based separators including polyacrylonitrile,²⁰⁻²² polyethylene terephthalate,²³ poly(butylene terephthalate),²⁴ polyvinylidene fluoride (PVdF) and its copolymer,²⁵⁻²⁸ polyimide,^{29,30} and polysulfonamide³¹ have been widely studied. PVdF nanofibers, in particular, have attracted significant attention because of their high dielectric constant and excellent anodic stability. However, the practical

use of electrospun PVdF separators is limited by their insufficient mechanical property (< 10 MPa), combined with the low heat resistance and poor thermal dimensional stability due to their low melting point (172 °C). Especially for the batteries used at high discharge rates or under severe conditions such as abnormal heating and mechanical shock.

Poly(*m*-phenylene isophthalamide) (PMIA) is a polymer with *meta*-type benzene-amide linkages in its skeletal chain (Fig. S1), thus leading to an extremely high thermal stability up to 400 °C,³² which can effectively avoid the short circuits caused by the shrinkage of the separators. Besides, the electrospun PMIA membranes show excellent mechanical strength of 31.34 MPa due to the inherent high-strength property of PMIA.³² Therefore, it is a potential strategy to overcome the above limitations of the electrospun PVdF membrane by introducing the PMIA fibers. To the best of our knowledge, no effort has succeeded because of the poor compatibility between them, and thus the integration of the PMIA with electrospun PVdF fibers is still a challenging problem and of great interest.

In the present work, we developed a sandwich structured PVdF/PMIA/PVdF composite separator for high power lithium ion battery, fabricating by a sequential electrospinning technique. We used the PVdF fibers as the shutdown layer, which could partially form closed pores to prevent the short circuit at elevated temperature. Key to our development design is that the use of PMIA fibers enabled to reinforce the mechanical strength and keep the integrity of separators after shutdown. By using the sandwich structured PVdF/PMIA/PVdF membranes, the composite separators exhibit excellent thermal stability, high ionic conductivity, desirable electrochemical stability, stable cycle performance, and prominent rate property, which are capable of providing robust battery performance for high power application.

Experimental

Materials

PVdF (HSV 900, Arkema) was purchased from Cndic Xiamen Imp. & Exp Co., Ltd., China. PMIA (Teijinconex®) was supplied by Teijin Ltd., Japan. *N,N*-dimethylacetamide (DMAc) was obtained from Shanghai Lingfeng Chemical Reagents Co., Ltd., China. Lithium chloride (LiCl) was purchased from Aladdin Industrial Co., China. The Celgard membrane (Celgard 2320, Celgard, China) with a thickness of about 20 μm were used as the separator for a comparative study. All chemicals were of analytical grade and used as received without further purification.

Fabrication of electrospun composite membranes

The LiCl/DMAc ionic liquid was used as the solvent for PMIA. The concentration of PMIA and LiCl in the precursor solution were 15 and 2 wt%, respectively. PVdF solution with a

concentration of 14 wt% was prepared by dissolving PVdF into DMAc for 14 h at room temperature. The representative setup for the preparation of PVdF/PMIA/PVdF composite separators was performed by using the DXES-3 spinning equipment (Shanghai Oriental Flying Nanotechnology Co., Ltd., China). The PVdF, PMIA, and PVdF solutions were sequentially electrospun onto the same target rotating collector, and the volume and flow rate for each solution were set as follows: (a) PVdF: 5 mL and 2 mL h^{-1} ; (b) PMIA: 1 mL and 0.1 mL h^{-1} ; (c) PVdF: 5 mL and 2 mL h^{-1} ; The spinning distance, voltage applied to the needle tip, processing temperature, and relative humidity were fixed at 25 cm, 30 kV, 23 ± 2 °C, and $45 \pm 3\%$, respectively. Then, the free-standing PVdF/PMIA/PVdF composite nanofibrous membranes were dried in a vacuum oven at 70 °C for 12 h to remove the residual solvent and transferred to a dry box for further use. The resultant PVdF/PMIA/PVdF membranes were denoted as V/M/V. For comparison, the single component of electrospun PVdF and PMIA nanofibrous membranes were also prepared according to the spinning conditions mentioned above.

Characterization

The morphology of the top surface and the cross section of relevant membranes was examined with high resolution field-emission scanning electron microscope (FE-SEM, S-4800, Hitachi Ltd., Japan) after sputtering a thin layer of gold. For the cross-section analysis, the composite membranes were subjected to brittle fracture in liquid nitrogen, and then the composite membranes were attached to the side wall of the sample table. The mechanical properties of the membranes were performed on a tensile tester (XQ-1C, Shanghai New Fiber Instrument Co., Ltd., China). The thermal properties of relevant membranes were evaluated by differential scanning calorimetry (DSC 200PC, Netzsch, Germany) at a heating rate of 10 °C min^{-1} from 50 to 260 °C under N_2 atmosphere. The mean pore size and pore size distribution of membranes were analyzed by a capillary flow porometer (Porometer 3Gzh, Quantachrome Instruments).

Porosity (P) was determined by immersing the dry membrane into *n*-butanol for 2 h until equilibrium was achieved at room temperature. The excess *n*-butanol adhering to the membrane surface was gently removed with wipes. The porosity of the membrane was calculated by the following equation:

$$P(\%) = \frac{M_{\text{BuOH}} / \rho_{\text{BuOH}}}{(M_{\text{BuOH}} / \rho_{\text{BuOH}}) + (M_m / \rho_p)} \times 100 \quad (1)$$

where M_m is the mass of the dry membrane, M_{BuOH} is the mass of *n*-butanol absorbed, ρ_{BuOH} and ρ_p are the densities of *n*-butanol and polymer, respectively.

Electrochemical performance evaluation

1 M lithium hexafluorophosphate (LiPF_6) dissolved in the mixed

solvent of ethylene carbonate (EC)/dimethyl carbonate (DMC)/ethyl methyl carbonate (EMC) (1/1/1, w/w/w) served as liquid electrolyte. Ionic conductivity (σ) of the electrospun separators was tested by AC impedance technique using the Zahner IM 6ex impedance analyzer. The impedance measurements were performed at an amplitude of 5 mV over the frequency range from 0.1 Hz to 1 MHz using the cell inserted separators into two stainless steel (SS) blocking electrodes. The ionic conductivity could be calculated from the following equation:

$$\sigma = \frac{d}{R_b \times S} \quad (2)$$

where d is the thickness of relevant nanofibrous membranes, which was measured by an electronic micrometer (0.001 mm accuracy, CHY-C2 Thickness Tester, Labthink Co. Jinan, China). R_b is the bulk resistance and S is the contact area between the separators and stainless steel blocking electrode. The electrochemical stability windows of the relevant separators were conducted by a linear sweep voltammetry (LSV), which was carried out on Li/separators/SS cell at a scan rate of 1 mV s⁻¹ over the potential range of 2.5-6.0 V vs. Li⁺/Li to check the oxidative decomposition.

Coin cells (2016-type) were assembled by sandwiching separators between the LiCoO₂ cathode (LiCoO₂/carbon black/PVdF, 90/5/5, w/w/w) and the lithium metal anode. The charge/discharge, cycle stability and C-rate capability of the cell were conducted in a Land battery test system (CT 2001A, Wuhan Land Electronic Co. Ltd., China) between 3.0 and 4.2 V at room temperature. All the assembly processes of cells were carried out in an argon-filled glovebox with oxygen and moisture level <1 ppm.

Results and discussion

Morphology

The representative FE-SEM images of PVdF membranes at different magnifications shown in Fig. 1a and b reveal that the as-spun membranes are composed of randomly oriented fibers with an average diameter of 367 nm. Interestingly, obvious adhesions could be observed among adjacent fibers (indicated by dotted circle), as shown in Fig. 1a. The formation of this structure could be attributed to the incomplete evaporation of DMAc. As can be seen in Fig. 1c, the diameter of PMIA nanofibers is uniform with an average size of around 100 nm. At a higher magnification (Fig. 1d), it can be seen that the surface of the electrospun PMIA membranes is smooth and almost free of beads, which is of vital importance for the mechanical performance of electrospun membranes. As seen from Fig. 1e, the composite membranes consist of three layers, the thin PMIA membranes is sandwiched by two layers of PVdF membranes. Meanwhile, the nanofibers of the PVdF layer and the PMIA layer are bonded and interconnected on the

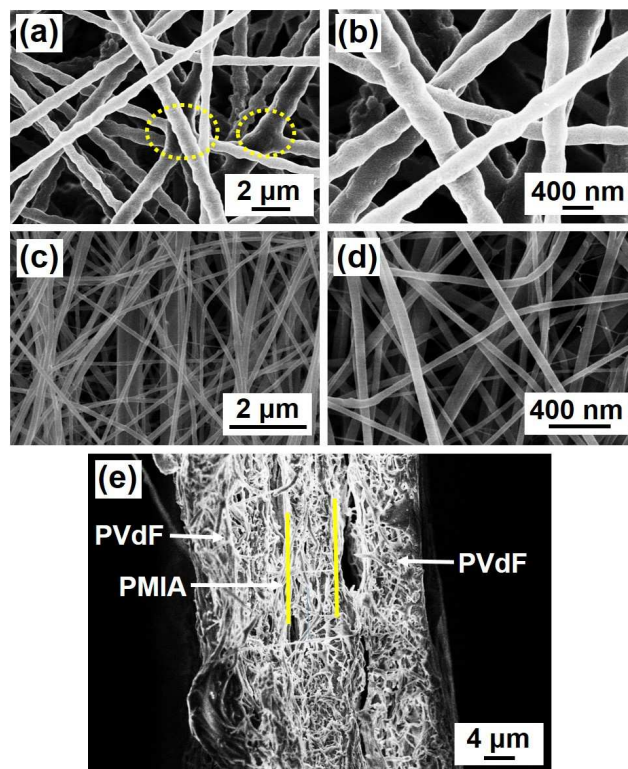


Fig. 1 FE-SEM images of (a and b) PVdF, (c and d) PMIA nanofibrous membranes. (e) FE-SEM image of the cross-section view of V/M/V composite membranes.

interface boundary. During the fabrication of the composite membranes, the PMIA nanofibers prefer to deposit on the interspace formed by the intersecting PVdF nanofibers due to the non-uniform electric field intensity,³³ and thus make them interconnected together. Moreover, the incomplete evaporation solvent at the fibres intersection points and extensive contact sites provided by the small diameter of nanometer scale make PVdF fibers bonded with PMIA fibers. The existence of the bonding structure is expected to play a key role in enhancing the mechanical property of the composite membranes.

Mechanical property

The typical stress-strain curves of PVdF, PMIA, and V/M/V composite membranes are shown in Fig. 2. It can be seen that the PMIA membranes exhibit a nonlinear elastic behavior in the first region under a stress load until reaching to the yield point, and then, the stress-strain curves displays a linear elastic behaviour with the continuous applied stress until break. This phenomenon could be explained by the two-step break mechanism. When a small external load is applied, the nonaligned nanofibers in membranes are forced to be aligned along the stress direction, resulting in the first nonlinear elastic behavior.³⁴ With the continual increase in tensile stress, the curve shows a linear elasticity due to the intrinsic property

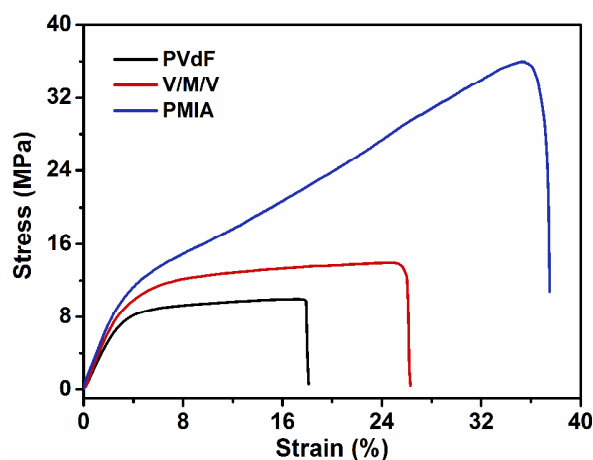


Fig. 2 Stress-strain curves of the as-prepared electrospun PVdF, V/M/V and PMIA nanofibrous membranes.

Table 1 Mechanical properties of relevant electrospun PVdF, V/M/V and PMIA nanofibrous membranes.

Samples	Breaking elongation (%)	Breaking stress (MPa)
PVdF	18.01 ± 0.82	9.97 ± 0.45
V/M/V	25.92 ± 1.05	13.96 ± 0.62
PMIA	35.51 ± 1.25	35.96 ± 1.06

of PMIA fibers. Finally, the break of the PMIA membranes results from the break of the individually aligned nanofibers.³⁵ The PVdF and V/M/V composite membranes show a non-linear elastic behavior in the first stage due to the slip of individual fibers,³⁶ and then the composite membranes show a non-linear elastic behavior in the stress-strain curves nearly reach a plateau stage. At this stage, the stress almost kept constant and the extension increased continuously before the membranes ruptured, which indicates that the slip of the relevant fibers has completed and the load is endured by the single oriented fiber along the direction of extension.³⁷ Finally, the break of relevant membranes is resulted from the break of fibers between the bonding points. The mechanical properties of the relevant electrospun nanofibrous membranes are summarized in Table 1. It is clearly shown that the tensile strength and elongation at break of the V/M/V composite membranes are 13.96 MPa and 46.09%, both of which are higher than those of pure PVdF membranes. This phenomenon could be due to the introduction of the high-strength PMIA fibers and the bonding structure formed between the adjacent layers. Consequently, the above results suggest that the V/M/V composite membranes possess robust mechanical property, which could be applied as promising materials for potential applications in lithium ion batteries.

Thermal stability

Thermal property of separators is a vital character that concerns

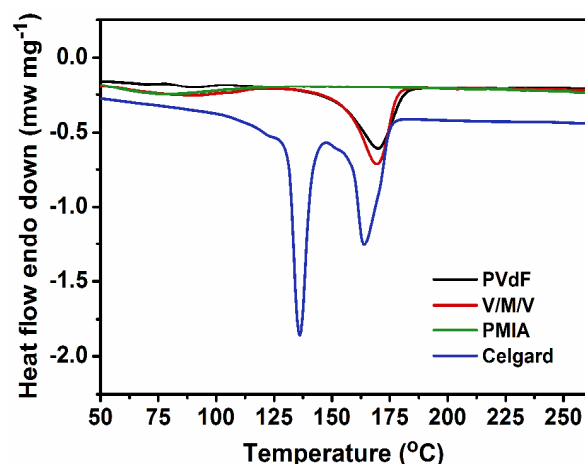


Fig. 3 DSC curves of Celgard membrane and the resultant electrospun PVdF, V/M/V, and PMIA nanofibrous membranes.

the safety characteristic of lithium ion battery. To evaluate the thermal properties, we conducted DSC measurements on the Celgard, PVdF, PMIA and V/M/V composite membranes (Fig. 3). It is observed that the Celgard membrane shows endothermic peaks at around 135 °C and 165 °C relating to the melting points of PE and PP, respectively, where the lower temperature endows the separator with shutdown characteristic at 135 °C. The PVdF nanofiber-based membranes shows an endothermic peak at 172 °C, which is the typical melting temperature of PVdF. Besides, the PMIA nanofibrous membranes exhibit thermal stability up to 260 °C except for an endothermic peak at 85 °C corresponding to the loss of absorbed water. All the above mentioned endothermic peaks exist in the V/M/V composite membranes, thus the PVdF fibers in the composite membranes could be responsible for the shutdown property of battery at 172 °C, which is beneficial for improving the thermal safety of the battery.

Thermal shrinkage of separators is another significant parameter to evaluate the safety performance of lithium ion battery. Fig. 4 a and b show the photographs of relevant separators before and after the hot oven tests at 180 °C for 1 h. The Celgard membrane shrinks seriously with the color change from white to transparent, and the PVdF membranes shrink by 25% due to its low melting point. Interestingly, for the as-spun PMIA and V/M/V composite membranes no shrinkage is observed, revealing the good heat resistance of the V/M/V composite membranes due to the introduction of high temperature tolerant PMIA. Apart from that, the morphology of the V/M/V membranes after being exposed to 180 °C for 1 h shown in Fig. 4c also gives a reasonably plausible explanation for the above results. The PVdF fibers in the V/M/V membranes exhibit melting features, which may result in the close up of the interconnected pores without deforming the integrity of the composite membranes. This prominent thermal stability could effectively prevent the thermal shrinkage of the

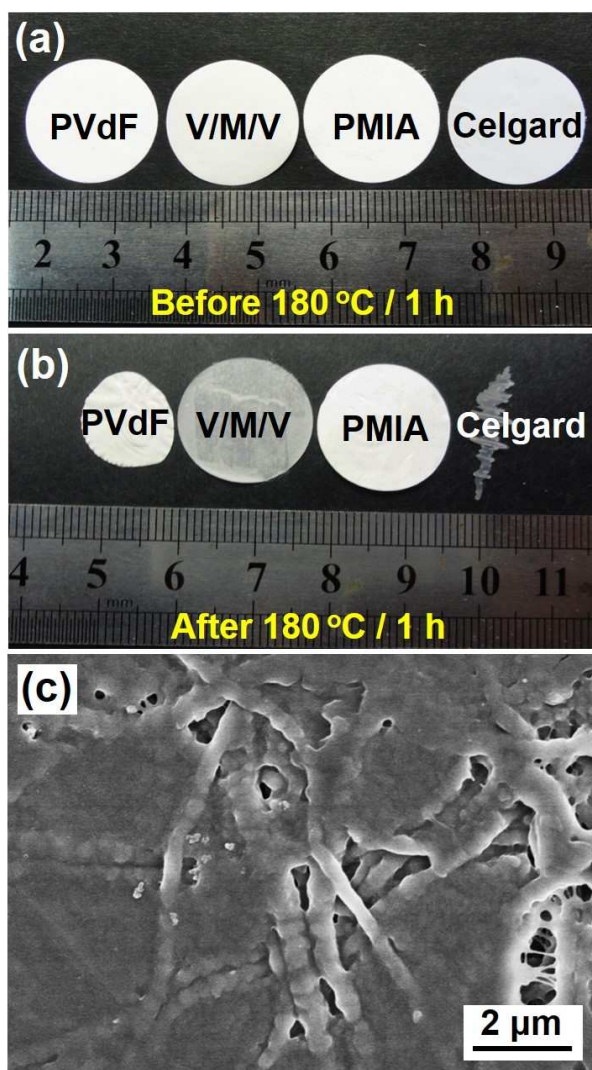


Fig. 4 Photographs of electrospun nanofibrous membranes and Celgard membrane (a) before and (b) after exposure to 180 °C for 1 h, (c) FE-SEM image of the composite membranes after being exposed to 180 °C for 1 h.

separators when a high charged/discharged rate is applied, which is beneficial for enhancing the safety performance of lithium ion battery.

Porous structure analysis

The capillary flow porometry method was used to measure the pore size of electrospun membranes and the wetting liquid (Porewick) with a surface tension of 16 dynes cm^{-1} was applied as the immersion solution. Fig. 5 shows the mean pore size and pore size distribution of electrospun PVdF, PMIA and V/M/V membranes before (a, b and c) and after (d, e and f) thermal treatment. It is worth noting that all types of the membranes have shown the pore size distribution in the range of 0.5-3.2 μm , the pore size distribution of the as-prepared composite membranes before and after heat treatment are uniform, which

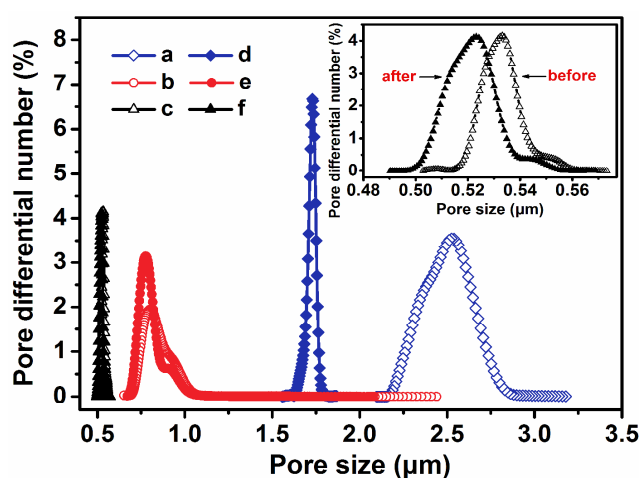


Fig. 5 Pore size distributions of electrospun PVdF (a and d), V/M/V (b and e), and PMIA (c and f) membranes before (a, b and c) and after (d, e and f) being exposed to 180 °C for 1 h. Inset shows the region (0.480-0.578 μm).

Table 2 Mean pore size, pore size distribution, and porosity of relevant electrospun nanofibrous membranes.

Samples	Mean pore size (μm)	Pore size distribution (μm)	Porosity (%)
PVdF	2.500	2.086-3.179	81.28
V/M/V	0.850	0.709-2.411	83.97
PMIA	0.532	0.514-0.570	90.90
Heat-treated PVdF	1.723	1.633-2.492	-
Heat-treated V/M/V	0.796	0.675-2.051	-
Heat-treated PMIA	0.520	0.496-0.554	-

can ensure a uniform current distribution throughout the separators. It is also clearly seen from Table 2 that the mean pore size of the resultant V/M/V composite membranes after being exposed to 180 °C for 1h decreases by 6.4%, while the mean pore size of the PMIA nanofibrous membranes shows little change. These results indicate that some of the pores in the V/M/V composite membranes close up after being exposed to 180 °C for 1 h, which are in good agreement with the above thermal stability analysis. The closed pores would hinder the conduction of lithium ion, hence decrease the ionic conductivity, and finally shut the cell down before an explosion occurs.³⁸ The fusion of the interconnected pores in the PVdF layers could endow the composite membranes with shutdown characteristic like polyolefin trilayer composite separator, which is beneficial for improving the safety performance of lithium ion battery.

Besides, porosity is another important factor that influences the ionic conductivity and electrochemical properties of separators. As shown in Table 2, the porosities of the prepared membranes vary in the range of 81.28-90.90%, which are higher than the value of Celgard membrane (49.83%). This phenomenon could be explained in the view of the distinctive

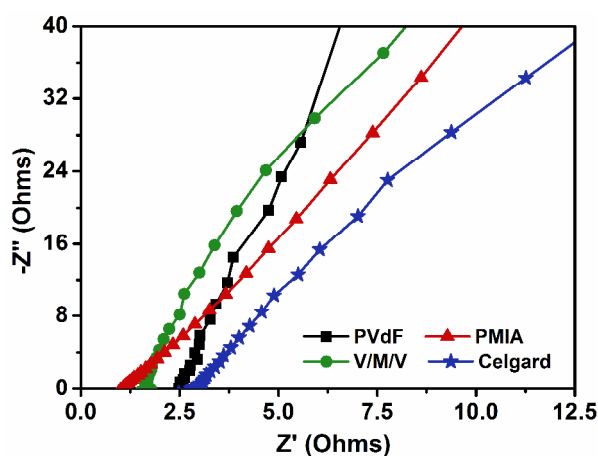


Fig. 6 AC impedance spectra of liquid electrolyte-soaked electrospun PVdF, V/M/V, PMIA nanofibrous membranes and Celgard membrane.

network structure of relevant membranes constructed by the electrospinning process. Moreover, the different porosities of relevant electrospun nanofibrous membranes could be attributed to the difference of the packing density of relevant membranes and the varied average fiber diameter (Fig. 1).

Ionic conductivity

Fig. 6 presents the Nyquist curves of the liquid electrolyte-soaked Celgard membrane and electrospun nanofibrous membranes determined by AC impedance at 20 °C. The conductivity can be obtained from the high-frequency intersection of the Nyquist curve on the Z' axis. The ionic conductivity of the as-prepared V/M/V composite membranes saturated with electrolyte can be up to 0.81 mS cm^{-1} , which is higher than that of the PVdF membranes (0.61 mS cm^{-1}) and Celgard membrane (0.35 mS cm^{-1}), but lower than that of the PMIA nanofibrous membranes (1.06 mS cm^{-1}). The ionic conductivity of the as-prepared V/M/V composite membranes is 2.3 times higher than that of the Celgard membrane, the relatively high ionic conductivity of the composite nanofibrous membranes can be attributed to its high porosity (Table 2), fully interconnected pore structure (Fig. 1), and the introduction of PMIA, indicating a noteworthy enhancement of the migration of lithium ions, and thus improve the rate performance of the battery.

Electrochemical stability

Electrochemical stability of the separators at the range of operating voltages of the battery system is very important for practical applications. Fig. 7 displays the anodic stability of liquid electrolyte-soaked electrospun membranes and the Celgard membrane, which are executed by linear sweep voltammetry up to 6.0 V at 20°C. The V/M/V composite membranes exhibit an anodic stability up to 5.15 V versus Li^+/Li , which is greater than the oxidation peak of the PMIA

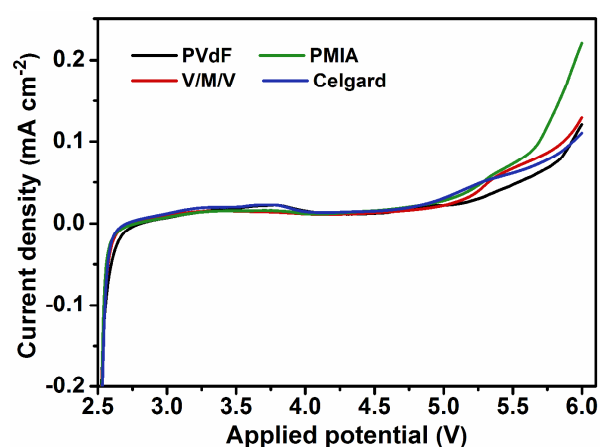


Fig. 7 Electrochemical stability windows of the cells with as-prepared PVdF, V/M/V, PMIA nanofibrous membranes and Celgard membrane.

membranes (5.10 V) and Celgard membrane (5.0 V), but lower than that of the PVdF membranes (5.20 V). The results reveal that the addition of the PMIA improves the porosity and ionic conductivity, and does not cause a negative effect on the electrochemical stability of the composite membranes. The decomposition voltage of 5.15 V could render the composite membranes potentially compatible with most high-voltage cathode materials used in rechargeable lithium ion batteries.

Battery performance

To demonstrate the applications of the resultant composite membranes in lithium ion battery, Li/LiCoO₂ coin cells using the composite membranes as separators were evaluated between 3.0 and 4.2 V at 20°C. For comparison, the cells using commercial Celgard membrane as separators were also tested. The discharge capacity as a function of cycle number of the cell subjected to 100 cycles is depicted in Fig. 8. It is clearly seen in

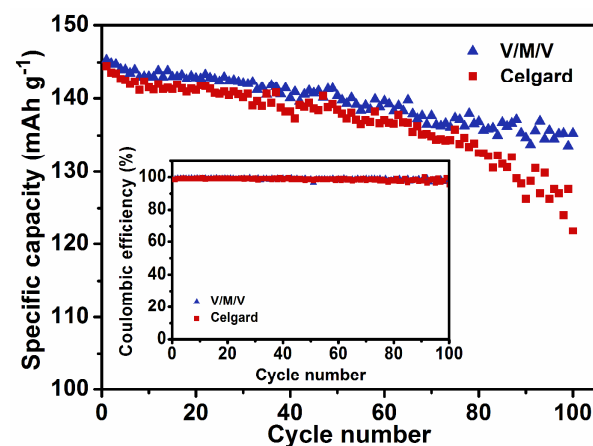


Fig. 8 Cycle performance of the cells assembled with the resultant composite membranes and Celgard membrane at 0.2C rate. Inset shows the coulombic efficiency as a function of the number of cycles.

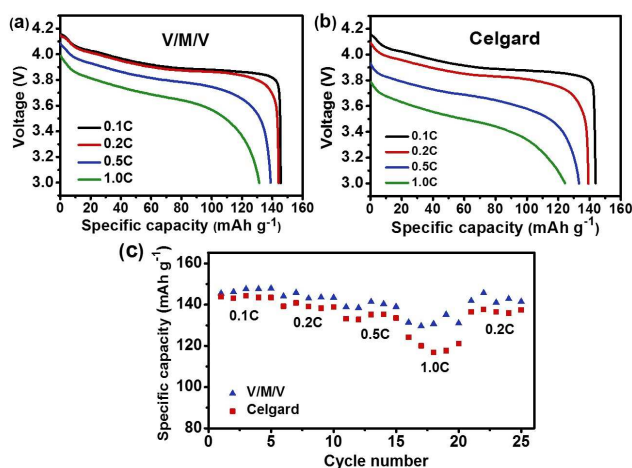


Fig. 9 Discharge curves of the cells assembled with (a) V/M/V composite membranes and (b) Celgard membrane as separators at different C-rate, (c) Comparison of the rate capabilities.

Fig. 8 that the obtained discharge capacity decreases with increasing the number of cycles, and the discharge capacity of the cell using the V/M/V membranes after 100 cycles is 135.29 mAh g⁻¹, which is 11% higher than that of Celgard membrane (121.85 mAh g⁻¹). The capacity retention ratio after 100th cycle of the cell with the composite membranes is 93.10%, while the cell with Celgard membrane shows only 84.34% capacity retention. Moreover, the cell with the resultant V/M/V composite membranes shows a comparable cycle life with a coulombic efficiency of nearly 100% (inset of Fig. 8). The remarkable improvement in the cycle property of the composite membranes may be caused by its high ionic conductivity (Fig. 6) attributing to its fully interconnected pore structure (Fig. 1).

The rate capabilities of the cells based on the composite membranes and Celgard membrane were measured by applying various current densities from 0.1C to 1.0C and back to 0.2C for 5 cycles each continuously. As can be seen in Fig. 9 a and b, the discharge capacities of the cells with the as-prepared V/M/V composite membranes and Celgard membrane gradually decrease with increasing C-rate. The discharge capacity and capacity retention (calculated based on the initial discharge capacity at 0.1C rate) of the as-prepared VM/V composite membranes are higher than those of Celgard membrane. Notably, the difference in discharge capacity becomes much larger when the charge/discharge current density up to 1.0C/1.0C, the composite membranes maintain 90% of the initial capacity obtained at 0.1C rate, while the Celgard membrane shows a low retention ratio of 83.75% of the initial value. When the rate returns to 0.2C after the rate test, the reversible discharge capacities of the cells with the composite and Celgard membranes were 142.86 and 137.52 mAh g⁻¹, respectively, which are very close to the original capacity of 0.2C rate (Fig. 9c). These results suggest that the

resultant composite membranes exhibit promising rate property, prominent rate capability, and good electrochemical stability, which are higher than those of the commercial Celgard membrane. Consequently, the above results showed that the V/M/V composite membranes possess excellent electrochemical performances, which could be applied as promising separators for a wide range of potential applications in lithium ion battery.

Conclusions

In summary, we have fabricated a novel kind of V/M/V composite membranes with shutdown characteristic via a sequential electrospinning technique as an advanced separator for high-performance lithium ion battery. The composite membranes consist of three layers, the thin PMIA membranes with an average fiber diameter of 100 nm is sandwiched by two layers of PVdF membranes with an average fiber diameter of 367 nm. The incorporation of the as-prepared PMIA fibers enabled the composite membranes to exhibit robust tensile strength of 13.96 MPa and high ionic conductivity up to 0.81 mS cm⁻¹ at 20 °C. The hot oven test indicated that the composite membranes exhibited no dimensional change even after being exposed to 180 °C for 1 h. Besides, the porous structure analysis revealed that the composite membranes indeed possessed shutdown function and could keep their integrity after closing the pores in the PVdF layer. More significantly, the cells based on the composite membranes demonstrate more stable cycling performance and better rate property compared with the commercial Celgard membrane, which match well with the requirements for application in safe, reliable and long lasting lithium batteries. This work provided a versatile strategy for the further design and development of robust mechanical strength and thermal stability separators for lithium ion battery.

Acknowledgments

This work is supported by the Shanghai Committee of Science and Technology (No. 12JC1400101), the National Natural Science Foundation of China (No. 51322304), the Fundamental Research Funds for the Central Universities, and the “DHU Distinguished Young Professor Program”. The Authors extend their appreciation to the Deanship of Scientific Research at King Saud University for funding the work through the international research group project No. IRG14-25.

Notes and references

^a State Key Laboratory for Modification of Chemical Fibers and Polymer Materials, College of Material Science and Engineering, Donghua University, Shanghai 201620, China. E-mail: binding@dhu.edu.cn (B. Ding)

^b College of Biological, Chemical Sciences and Engineering, Jiaying University, Jiaying 314001, China

^c College of Textiles, Donghua University, Shanghai 201620, China

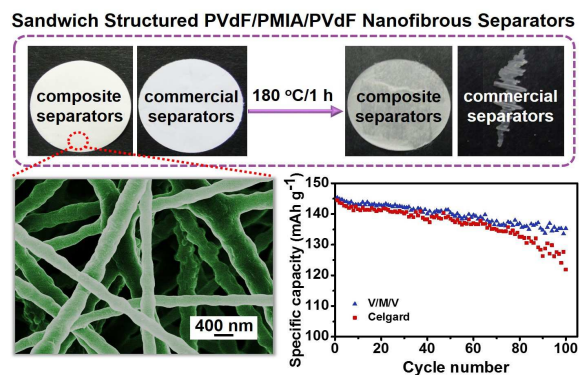
^d Petrochemical Research Chair, Department of Chemistry, College of Science, King Saud University, Riyadh 11451, Saudi Arabia

^e Department of Chemistry, Faculty of Science, Tanta University, Tanta 31527, Egypt

† Electronic Supplementary Information (ESI) available: Chemical structure of PMIA and the initial charge-discharge curves of the cells with the composite membranes and Celgard membrane as separators at 0.1C rate. See DOI: 10.1039/b000000x/

- 1 J. B. Goodenough and K. S. Park, *J. Am. Chem. Soc.*, 2013, **135**, 1167-1176.
- 2 V. Etacheri, R. Marom, R. Elazari, G. Salitra and D. Aurbach, *Energy Environ. Sci.*, 2011, **4**, 3243-3262.
- 3 Q. Wang, P. Ping, X. Zhao, G. Chu, J. Sun and C. Chen, *J. Power Sources*, 2012, **208**, 210-224.
- 4 P. Arora and Z. Zhang, *Chem. Rev.*, 2004, **104**, 4419-4462.
- 5 S. S. Zhang, *J. Power Sources*, 2007, **164**, 351-364.
- 6 W. C. Yu, *U. S. Pat.*, 6 878 226, 2005.
- 7 B. Schmitz and D. Busch, *U.S. Pat.*, 0 244 306, 2010.
- 8 T. H. Cho, M. Tanaka, H. Onishi, Y. Kondo, T. Nakamura, H. Yamazaki, S. Tanase and T. Sakai, *J. Electrochem. Soc.*, 2008, **155**, A699-A703.
- 9 J. Zhang, Z. Liu, Q. Kong, C. Zhang, S. Pang, L. Yue, X. Wang, J. Yao and G. Cui, *ACS Appl. Mater. Interfaces*, 2013, **5**, 128-134.
- 10 J. Liu, W. Li, X. Zuo, S. Liu and Z. Li, *J. Power Sources*, 2013, **226**, 101-106.
- 11 Y. S. Jung, A. S. Cavanagh, L. Gedvilas, N. E. Widjonarko, I. D. Scott, S. H. Lee, G. H. Kim, S. M. George and A. C. Dillon, *Adv. Energy Mater.*, 2012, **2**, 1022-1027.
- 12 J. Shi, H. Hu, Y. Xia, Y. Liu and Z. Liu, *J. Mater. Chem. A*, 2014, DOI: 10.1039/C4TA00808A.
- 13 S. J. Chun, E. S. Choi, E. H. Lee, J. H. Kim, S. Y. Lee and S. Y. Lee, *J. Mater. Chem.*, 2012, **22**, 16618.
- 14 Y. Zhu, S. Xiao, Y. Shi, Y. Yang and Y. Wu, *J. Mater. Chem. A*, 2013, **1**, 7790-7797.
- 15 B. Ding, M. Wang, X. Wang, J. Yu and G. Sun, *Mater. Today*, 2010, **13**, 16-27.
- 16 J. Lin, X. Wang, B. Ding, J. Yu, G. Sun and M. Wang, *Crit. Rev. Solid State Mater. Sci.*, 2012, **37**, 94-114.
- 17 X. Wang, B. Ding, G. Sun, M. Wang and J. Yu, *Prog. Mater. Sci.*, 2013, **58**, 1173-1243.
- 18 X. Wang, B. Ding and B. Li, *Mater. Today*, 2013, **16**, 229-241.
- 19 S. Cavaliere, S. Subianto, I. Savych, D. J. Jones and J. Rozière, *Energy Environ. Sci.*, 2011, **4**, 4761-4785.
- 20 Y. Liang, Z. Lin, Y. Qiu and X. Zhang, *Electrochim. Acta*, 2011, **56**, 6474-6480.
- 21 P. C. Lee, T. H. Han, T. Hwang, J. S. Oh, S. J. Kim, B. W. Kim, Y. Lee, H. R. Choi, S. K. Jeoung, S. E. Yoo and J. D. Nam, *J. Membr. Sci.*, 2012, **409-410**, 365-370.
- 22 Y. J. Kim, H. S. Kim, C. H. Doh, S. H. Kim and S. M. Lee, *J. Power Sources*, 2013, **244**, 196-206.
- 23 J. Hao, G. Lei, Z. Li, L. Wu, Q. Xiao and L. Wang, *J. Membr. Sci.*, 2013, **428**, 11-16.
- 24 C. J. Orendorff, T. N. Lambert, C. A. Chavez, M. Bencomo and K. R. Fenton, *Adv. Energy Mater.*, 2013, **3**, 314-320.
- 25 S. W. Choi, J. R. Kim, Y. R. Ahn, S. M. Jo and E. J. Cairns, *Chem. Mater.*, 2007, **19**, 104-115.
- 26 F. Zhang, X. Ma, C. Cao, J. Li and Y. Zhu, *J. Power Sources*, 2014, **251**, 423-431.
- 27 P. Raghavan, X. Zhao, C. Shin, D. H. Baek, J. W. Choi, J. Manuel, M. Y. Heo, J. H. Ahn and C. Nah, *J. Power Sources*, 2010, **195**, 6088-6094.
- 28 F. Croce, M. L. Focarete, J. Hassoun, I. Meschini and B. Scrosati, *Energy Environ. Sci.*, 2011, **4**, 921-927.
- 29 J. Ding, Y. Kong, P. Li and J. Yang, *J. Electrochem. Soc.*, 2012, **159**, A1474-A1480.
- 30 Y. E. Miao, G. N. Zhu, H. Hou, Y. Y. Xia and T. Liu, *J. Power Sources*, 2013, **226**, 82-86.
- 31 X. Zhou, L. Yue, J. Zhang, Q. Kong, Z. Liu, J. Yao and G. Cui, *J. Electrochem. Soc.*, 2013, **160**, A1341-A1347.
- 32 J. Lin, B. Ding, J. Yang, J. Yu and S. S. Al-Deyab, *Mater. Lett.*, 2012, **69**, 82-85.
- 33 D. Zhang and J. Chang, *Adv. Mater.*, 2007, **19**, 3664-3667.
- 34 X. Wang, Y. Si, X. Wang, J. Yang, B. Ding, L. Chen, Z. Hu and J. Yu, *Nanoscale*, 2013, **5**, 886-889.
- 35 X. Tang, Y. Si, J. Ge, B. Ding, L. Liu, G. Zheng, W. Luo and J. Yu, *Nanoscale*, 2013, **5**, 11657-11664.
- 36 N. Wang, A. Raza, Y. Si, J. Yu, G. Sun and B. Ding, *J. Colloid Interface Sci.*, 2013, **398**, 240-246.
- 37 J. Lin, F. Tian, Y. Shang, F. Wang, B. Ding, J. Yu and Z. Guo, *Nanoscale*, 2013, **5**, 2745-2755.
- 38 M. Xiong, H. Tang, Y. Wang, Y. Lin, M. Sun, Z. Yin and M. Pan, *J. Power Sources*, 2013, **241**, 203-211.

Graphical abstract



Novel, sandwich structured PVdF/PMIA/PVdF nanofibrous battery separators with robust mechanical strength and thermal stability are fabricated via a sequential electrospinning technique.